Protein Expression and Purification 93 (2014) 23–31

Contents lists available at ScienceDirect

Protein Expression and Purification

journal homepage: www.elsevier.com/locate/yprep

Novel high-performance purification protocol of recombinant CNBP suitable for biochemical and biophysical characterization

Emilse Challier [a], María-Natalia Lisa [a,b], Bibiana B. Nerli [c], Nora B. Calcaterra [a], Pablo Armas [a,*]

[a] Instituto de Biología Molecular y Celular de Rosario (IBR), Consejo Nacional de Investigaciones Científicas y Técnicas (CONICET) – Facultad de Ciencias Bioquímicas y Farmacéuticas, Universidad Nacional de Rosario, CCT-Rosario, Ocampo y Esmeralda, S2000FHQ Rosario, Argentina
[b] Institut Pasteur, Unité de Microbiologie Structurale, CNRS URA 2185, 25 rue du Docteur Roux, 75724 Paris, France
[c] Departamento Química-Física, Facultad de Ciencias Bioquímicas y Farmacéuticas, Universidad Nacional de Rosario, Suipacha 531, S2002LRK Rosario, Argentina

ARTICLE INFO

Article history:
Received 16 September 2013
Available online 22 October 2013

Keywords:
Cellular nucleic acid binding protein
Zinc knuckle
Tag-free
Nucleic acid binding
Intrinsic fluorescence quenching
Proteolysis assay
Intrinsically unstructured protein

ABSTRACT

Cellular nucleic acid binding protein (CNBP) is a highly conserved multi-zinc knuckle protein that enhances *c-MYC* expression, is related to certain human muscular diseases and is required for proper rostral head development. CNBP binds to single-stranded DNA (ssDNA) and RNA and acts as nucleic acid chaperone. Despite the advances made concerning CNBP biological roles, a full knowledge about the structure–function relationship has not yet been achieved, likely due to difficulty in obtaining pure and tag-free CNBP. Here, we report a fast, simple, reproducible, and high-performance expression and purification protocol that provides recombinant tag-free CNBP from *Escherichia coli* cultures. We determined that tag-free CNBP binds its molecular targets with higher affinity than tagged-CNBP. Furthermore, fluorescence spectroscopy revealed the presence of a unique and conserved tryptophan, which is exposed to the solvent and involved, directly or indirectly, in nucleic acid binding. Size-exclusion HPLC revealed that CNBP forms homodimers independently of nucleic acid binding and coexist with monomers as non-interconvertible forms or in slow equilibrium. Circular dichroism spectroscopy showed that CNBP has a secondary structure dominated by random-coil and β-sheet coincident with the sequence-predicted repetitive zinc knuckles motifs, which folding is required for CNBP structural stability and biochemical activity. CNBP structural stability increased in the presence of single-stranded nucleic acid targets similar to other unstructured nucleic acid chaperones. Altogether, data suggest that CNBP is a flexible protein with interspersed structured zinc knuckles, and acquires a more rigid structure upon nucleic acid binding.

Introduction

Cellular nucleic acid binding protein (CNBP)[1], also called zinc-finger protein 9 (ZNF9), is a highly conserved single-stranded nucleic acid-binding protein containing seven CCHC-type zinc knuckles. It is involved in the myotonic dystrophy type 2 (DM2) [1,2] and age-related sporadic inclusion body myositis (sIBM) [3] human muscular diseases; in systemic lupus erythematosus [4]; as well as in rostral head development [5–7].

CNBP mainly consists of seven CCHC zinc knuckles and an RGG box domain located between the first and second zinc knuckles (Fig. 1A) [8,9]. This protein binds to single-stranded DNA (ssDNA) and RNA [10,11], participating in the control of transcriptional and translational processes [12–17]. Through the control of the expression of its targets, CNBP seems to govern cell death and proliferation rates [18].

Despite the knowledge on CNBP biological features markedly increased in last years, scant information exists concerning its biochemical and structural properties. So far, CNBP biochemical characterizations have been done using recombinant CNBP fused to different protein tags; e.g., His_6 or GST [4,8,10,19–26]. It was shown that CNBP binds RNA and ssDNA with similar affinities, but it does not bind double-stranded DNA; binds RNA mainly as a dimer while either monomer or dimer can bind ssDNA, and; prefers G-rich unpaired stretches as targets [10,11]. In addition, CNBP-tagged proteins allowed the characterization *in vitro* of CNBP as nucleic acid chaperone [10,21,22].

* Corresponding author. Address: IBR – CONICET, CCT-Rosario, Ocampo y Esmeralda, S2000FHQ Rosario, Santa Fe, Argentina. Tel./fax: +54 341 4237070x654.
E-mail addresses: armas@ibr-conicet.gov.ar, parmas@fbioyf.unr.edu.ar (P. Armas).

[1] *Abbreviations used:* CNBP, cellular nucleic acid binding protein; ZNF9, zinc-finger protein 9; CCHC, Cys-Cys-His-Cys; RGG, Arg-Gly-Gly; ssDNA, single-stranded DNA; GST, glutathione-*S*-transferase; FMRP, fragile X mental retardation protein; NCp, nucleocapsid protein; Trx, thioredoxin; TEV, tobacco etch virus; LB, Luria–Bertani medium; LB-Zn, LB medium supplemented with 0.3 mM $ZnCl_2$; EMSA, electrophoretic mobility shift assay; K_d, dissociation constant; K_a, association constant; K_S, Stern–Volmer constant of static quenching; K_D, Stern–Volmer constant of dynamic quenching; CD, circular dichroism; NCp, nucleocapsid protein; OD_{600nm}, optical density at 600 nm; IPTG, isopropil-β-D-thio galactopyranoside; EDTA, ethylenediaminetetraacetic acid.

1046-5928/$ - see front matter © 2013 Elsevier Inc. All rights reserved.
http://dx.doi.org/10.1016/j.pep.2013.10.006

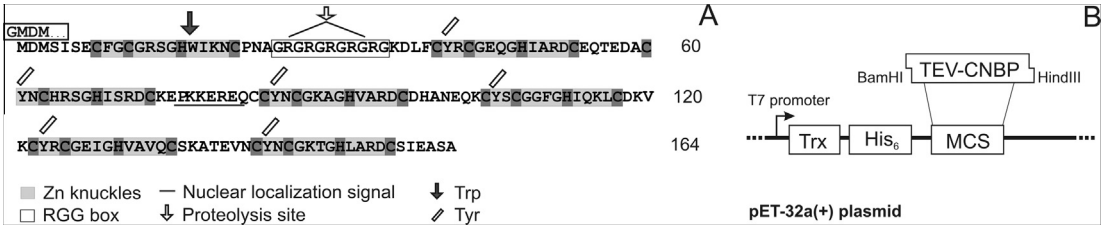

Fig. 1. CNBP primary structure and cloning strategy. (A) Zebrafish CNBP primary structure showing its main structural features. Amino acids sequence determined by N-terminus automated Edman degradation is boxed above the primary sequence. (B) Scheme of the expression system using pET-32a(+) plasmid. CNBP cDNA was introduced as a thioredoxin translational fusion separated by an His_6 linker and the specific TEV protease site to obtain the Trx-His_6-TEV-CNBP fusion protein.

The use of tags is often advantageous for purifying recombinant proteins; however, the presence of such tags might affect the structure and function of proteins [27]. Due to these negative effects, different methods for the specific removal of these tag sequences have been developed. Most of them include chemical cleavage into the chimeric protein and using commercially available proteases to remove the tag [27]. However, most of the commonly used proteases recognize a putative proteolysis site located between the first and second CCHC domain in CNBP, thus impairing the purification of homogeneously pure full-length isoform (unpublished data). This proteolysis generates a shorter isoform that losses nucleic acid chaperone activity and displays different nucleic acid binding behavior [8,21].

We report here the set-up of a fast, simple and reproducible protocol to purify homogeneously pure, active, and tag-free full-length CNBP. In addition, this protocol yields large quantities of protein, thus allowing getting insight into the CNBP biochemical and structural features. Using tag-free CNBP we found that CNBP is a flexible and unstructured protein with interspersed structured zinc knuckles, which forms homodimers autonomously and becomes more resistant to proteolysis, probably through a more rigid structure, upon nucleic acid binding.

Materials and methods

Plasmid construction

Zebrafish (*Danio rerio*) CNBP cDNA, GenBank N° AY228240 [20] was PCR amplified with primers Fwd: 5′-CGC GGA TCC GAA AAC CTG TAT TTT CAG GGC ATG GAC ATG AGT ACC AGT GAG-3′ and Rev: 5′-CCC AAG CTT CTA CGC GGA CGC TTC GAT-3′. Fwd primer contained the BamHI restriction site, the coding sequence for the peptide Glu-Asn-Leu-Tyr-Phe-Gln-Gly specifically recognized by the tobacco etch virus (TEV) protease [28,29], and the first CNBP methionine ATG codon. Rev primer contained the HindIII restriction site and the CNBP stop TAG codon. The BamHI and HindIII digested PCR product was cloned into pET-32a(+) expression vector (Novagen, Inc.) obtaining the pET-32-TEV-CNBP plasmid, which encodes a thioredoxin(Trx)-His_6-TEV-CNBP fusion protein.

Expression of recombinant CNBP

Escherichia coli BL-21 (DE3) was transformed with pET-32-TEV-CNBP plasmid and cultured in Luria–Bertani medium (LB) supplemented with 100 μg/ml ampicillin. In the case of culture medium supplemented with Zn^{2+} (LB-Zn) 0.3 mM $ZnCl_2$ was added. Cultures grown at 37 °C up to OD_{600nm} of 0.5–0.6 were induced adding 0.5 mM IPTG and cultured for 6 h at 37 °C. Bacteria were collected by centrifugation and pellets were resuspended in Lysis Buffer (50 mM Tris–HCl pH 7.5; 300 mM NaCl, 10 mM Imidazole; 10 mM β-mercaptoethanol; 10% Glycerol and 1% Protease Inhibitor Cocktail – Sigma Catalog #P8340). Cells were lysated by sonication at 4 °C and centrifuged for 15 min at 4 °C at 100,000*g*, obtaining soluble proteins in the supernatant.

Affinity purification chromatography

Supernatant containing Trx-His_6-TEV-CNBP was filtered through a 0.45 μm membrane and loaded into a HisTrap Fast Flow column (GE Healthcare) Ni^{2+}-column equilibrated in Buffer A (50 mM Tris–HCl pH 7.5; 300 mM NaCl; 30 mM Imidazole; 10% Glycerol and 10 mM β-mercaptoethanol). The column was washed once with 3 column volumes of 6% of Buffer B (50 mM Tris–HCl pH 7.5; 300 mM NaCl; 500 mM Imidazole; 10% Glycerol and 10 mM β-mercaptoethanol) in Buffer A, and once with 3 column volumes of 8% Buffer B in Buffer A. Finally, Trx-His_6-TEV-CNBP fusion was eluted with 100% of Buffer B. Protein concentration was estimated by densitometry analysis of Coomassie Brilliant Blue stained SDS–PAGE gels as described elsewhere [10]. Afterwards, Trx-His_6-TEV-CNBP fusion was treated with recombinant His_6-TEV protease in a His_6-TEV/Trx-His_6-TEV-CNBP ratio of 1:40, and dialyzed overnight in Dialysis Buffer I (50 mM Tris–HCl pH 7.5; 300 mM NaCl; 1 mM DTT and 0.1 mM $ZnCl_2$). Subsequently, CNBP was purified in batch using Ni–NTA agarose resin (Qiagen). His_6-polypeptides were allowed to bind to the matrix for 4 h at 4 °C and gentle agitation and CNBP was recovered in the resin flow-through fraction. All purification steps were performed at 4 °C.

Anion exchange chromatography

Affinity purified CNBP was dialyzed in Dialysis Buffer II (50 mM Tris–HCl pH 6.5; 10% Glycerol and 5 μM $ZnCl_2$) and filtered through a 0.45 μm membrane. The filtrate was loaded into an anion exchange chromatography column using Q-Sepharose™ Fast Flow resin (GE Healthcare) equilibrated with Equilibration and Wash Buffer (50 mM Tris–HCl pH 6.5; 10% Glycerol and 5 μM $ZnCl_2$). Elution was made by a three-step-gradient of NaCl (100, 200, and 500 mM) in Equilibration and Wash Buffer. All purification steps were performed at 4 °C.

Protein analysis

Protein concentration was determined by absorbance at 280 nm using a calculated molar extinction coefficient of 16010 M^{-1} cm^{-1} for CNBP, which was estimated according to Gill and von Hippel [30]. Electronic absorption spectra were recorded on a Jasco V-630 spectrophotometer, at 25 °C, in the corresponding elution buffers and in protein concentrations ranging from 5 to 30 μM. Protein electrophoreses (15% SDS–PAGE) and western blots were performed as described elsewhere [5,8,31], using 1:2000 diluted anti-CNBP antiserum (raised in rabbits), 1:3000 diluted anti-His_6 antibody (monoclonal, GE Healthcare Cat. #27-4710-01), and 1:5000 diluted anti-rabbit or anti-mouse antibodies coupled to horseradish peroxidase (HRP) (GE Healthcare), and

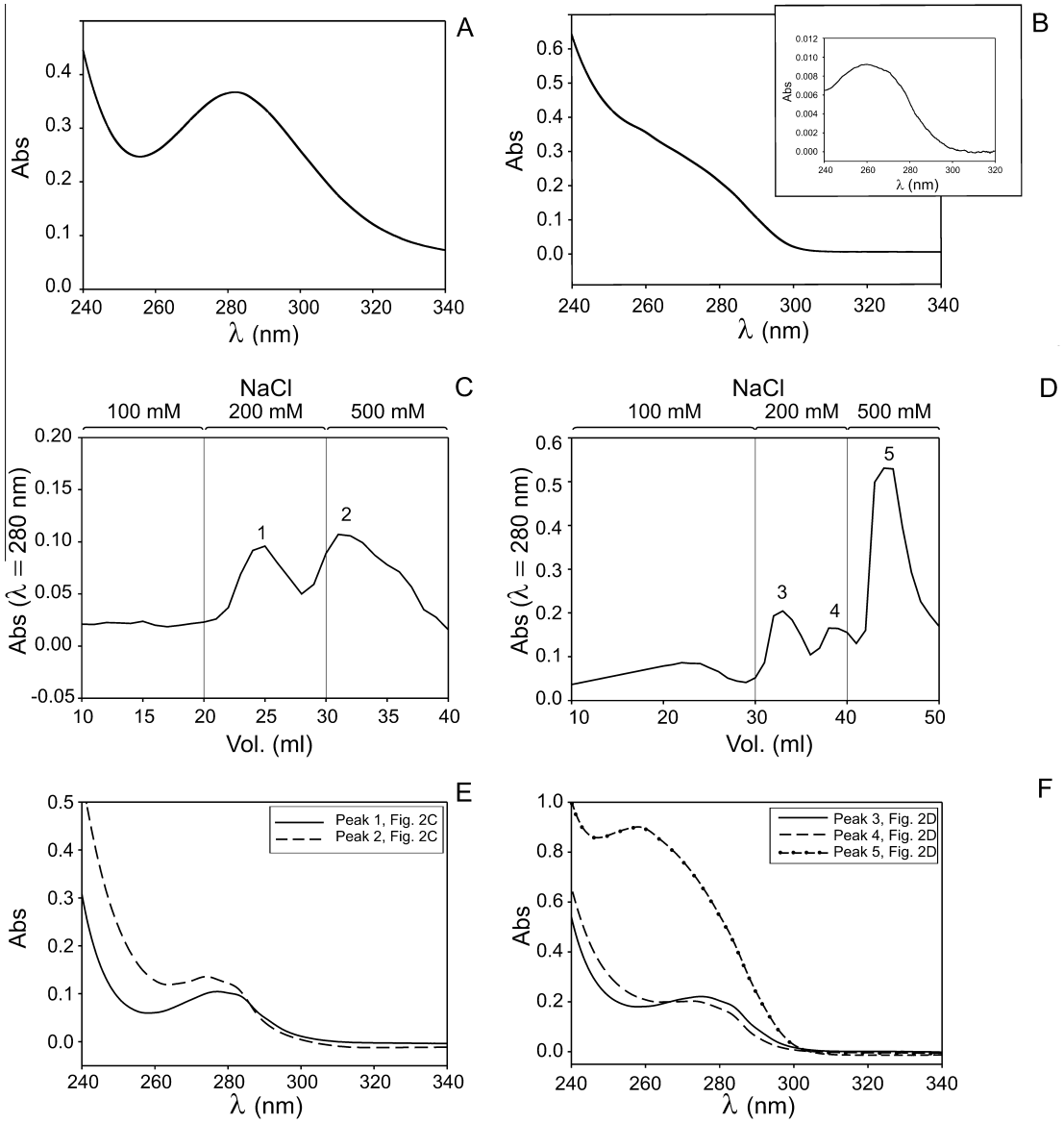

Fig. 2. Electronic absorption spectra of CNBP purified in different experimental conditions. Absorption spectra of purified CNBP-LB (A) and CNBP-LB-Zn (B). Inset shows the absorption spectrum of the nucleic acids obtained after phenol:chloroform extraction and ethanol precipitation of purified CNBP-LB-Zn. Elution profiles (280 nm absorbance) of anion exchange chromatographies of CNBP-LB (C) and CNBP-LB-Zn (D). Ionich strength changes (NaCl concentration) are indicated at the top of the elution profiles. Absorption spectra of peaks 1 and 2 of CNBP-LB (E) and peaks 3, 4 and 5 of CNBP-LB-Zn (F).

chemiluminescence was detected using SuperSignal West Pico Chemiluminescent Substrate (Pierce). N-terminal sequencing of purified recombinant CNBP was performed by loading the protein sample on 18% SDS–PAGE, transfering to Hybond-P PVDF membrane (GE Healthcare) and staining with Amido Black. The band corresponding to CNBP (≈18 kDa) was cut-off and subjected to N-terminus sequencing by automated Edman degradation in the LANAIS-PRO service (Instituto de Química y Fisicoquímica Biológicas, Facultad de Farmacia y Bioquímica, Universidad de Buenos Aires, Argentina).

Zinc quantification

CNBP Zn^{2+} content was determined by atomic absorption spectroscopy using a Metrolab 250 AA instrument operating in the flame mode. Measurements were performed on protein samples obtained after the second dialysis step in a buffer containing 5 μM $ZnCl_2$. The metal content of the dialysis buffer was subtracted from that of the protein sample in each case. Zinc atomic absorption standard (995 ppm – Sigma Catalog #Z-2750) was used for calibration curves.

Electrophoretic mobility shift assay (EMSA)

Electrophoretic mobility shift assays and apparent dissociation constants (K_d) estimations were performed as previously described [10,21]. Probes sequences were the same as used elsewere [8,10]: sRNA-L4-UTR (43 b) 5′-CCU UUU CUC UUC GUG GCC GCU GUG GAG AAG CAG CGA GGA GAU G-3′ and Comp-CT (45 b) 5′-TTT GGG AAC CCG GGA GGG GCG CTT ATG GGG TGG GTG-3′. Zinc relevance in CNBP nucleic acid binding activity was analyzed by incubation of 5 μM recombinant proteins with 10 mM EDTA for 30 min at 37 °C prior to the incubation with nucleic acids.

Fluorescence spectroscopy

Intrinsic tryptophan fluorescence was measured with a Varian Cary Eclipse Fluorescence spectrophotometer using a 1 cm light path. For quenching titrations, excitation wavelength was set to

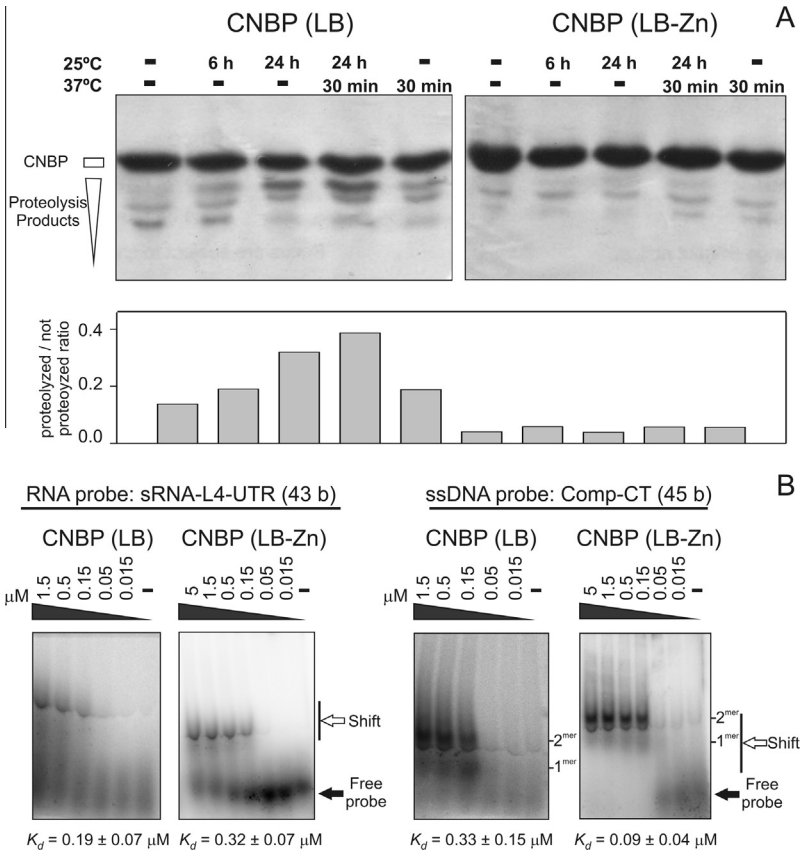

Fig. 3. Structural stability and biochemical functionality of purified CNBP. (A) CNBP structural stability was evaluated by spontaneous proteolysis incubating recombinant purified CNBP-LB and CNBP-LB-Zn for different periods of time at 25 or 37 °C and then analyzing the proteolysis products by Coomassie Brilliant Blue stained SDS–PAGE. Proteolyzed/not proteolyzed ratios were calculated from the densitometric intensity of SDS–PAGE bands. (B) EMSAs were done using labeled RNA (sRNA-L4-UTR) or ssDNA (Comp-CT) probes and increasing amounts of CNBP-LB or CNBP-LB-Zn. Free and shifted probes are indicated by arrows at the right of the gels. For the ssDNA probe, complexes are indicated as 1^{mer} (monomer) or 2^{mer} (dimer). The ssDNA free probe was allowed to escape from the gel of CNBP-LB (left gel) during electrophoresis in order to separate the shifted bands more efficiently. Dissociation constants were calculated from the intensity of the radioactive bands of free probes and complexes (Fig. S2 in Supplementary Material).

Table 1
Apparent dissociation constants (K_d) calculated with different CNBP forms.

	CNBP (LB-Zn) (Fig. 3B and Fig. S2)	CNBP (LB) (Fig. 3B and Fig. S2)	GST-CNBP (Fig. S3)
RNA	0.32 ± 0.07[a]	0.19 ± 0.07[b]	0.51 ± 0.07[c]
ssDNA	0.09 ± 0.04[d]	0.33 ± 0.15[e]	0.57 ± 0.09[f]

All calculated apparent dissociation constants are expressed in μM units.
[c] is statistically different from [a] and [b] ($p < 0.05$, *t*-student test).
[f] is statistically different from [d] and [e] ($p < 0.05$, fisher LSD method).
[d] is statistically different from [e] ($p < 0.05$, fisher LSD method).

295 nm and emission was recorded as the average value obtained for the 352–357 nm wavelength range in the spectra at each titration point. Quenching titrations were performed using a 3 μM CNBP solution in 15 mM Tris–HCl pH 7.5, 60 mM NaCl, 3% Glycerol and 1.5 μM $ZnCl_2$. Iodide quenching was performed adding increasing volumes of a 1.5 M NaI stock solution up to 100 mM final concentration. Increasing volumes of 10 μM RNA probe (sRNA-L4-UTR) and 10 μM of ssDNA probe (Comp-CT) stock solutions were added up to 500 nM final concentrations for titrations with nucleic acids. Fluorescence values were corrected for background fluorescence of the buffer, for dilution during titrations, and for inner filter.

Analysis of fluorescence quenching data

Fluorescence quenching experiments were analyzed by plots of relative fluorescence (F/F_0) vs. quencher concentration, and Stern–Volmer plots (F_0/F vs. quencher concentration) to obtain by linear regression the slopes which represented the Stern–Volmer quenching constants. Relative quenching ΔF data (F_0-F/F_0) were plotted vs. nucleic acid concentration and non-linearly fitted by assuming a binding model of equivalent and independent protein binding sites to calculate association constants (K_a) [32]. Graphical plots, linear regressions and iterative non-linear function fitting were performed using SigmaPlot 10.0 software (Systat Software, Inc.).

Size exclusion chromatography

A purified 3 μM CNBP sample was analyzed in a size exclusion chromatography (Zorbax GF-450 HPLC column) in 50 mM Tris–HCl pH 6.5, 10% Glycerol, 200 mM NaCl and 5 μM $ZnCl_2$. The molecular weight of each peak was assigned by interpolation in the profile of standards of known molecular masses (BSA and Carbonic Anhydrase). Alternatively, CNBP was pre-incubated for 30 min with 0.5 μM nucleic acid as indicated, and then analyzed by HPLC size exclusion chromatography.

Circular dichroism spectroscopy

Circular dichroism (CD) spectra were recorded at room temperature, in the 200–280 nm wavelength range, using a Jasco-810 spectropolarimeter with a scanning speed of 100 nm/min in a quartz cell of 1 cm optical path-length. Protein concentration was

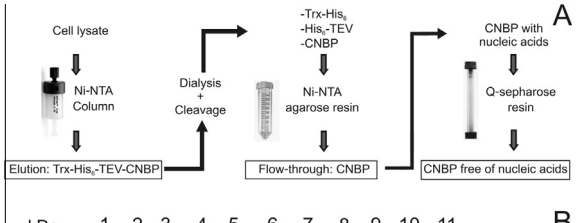

C

	*Trx-CNBP$_1$	*Trx-CNBP$_2$	CNBP$_1$	CNBP$_2$	CNBP$_3$
1 L Culture	55 mg 0.85 mg/ml	50 mg 1.35 mg/ml	25 mg 0.5 mg/ml	20 mg 0.4 mg/ml	5 mg 0.2 mg/ml

Fig. 4. CNBP purification strategy, analysis and yield. (A) Scheme of CNBP whole purification procedure. Two steps of Ni^{2+} affinity chromatography were performed separated by TEV digestion, followed by a final step of anion exchange chromatography. (B) Coomassie Brilliant Blue stained SDS–PAGE of the zebrafish CNBP purification steps: soluble (lane 1) and insoluble (lane 2) induced culture extracts, first Ni^{2+} chromatography flow-through (lane 3), first wash (lane 4), second wash (lane 5) and elution (lane 6); soluble (lane 7) and insoluble (lane 8) products of TEV digestion; soluble (lane 9) and insoluble (lane 10) flow-through of the second Ni^{2+} chromatography. Lane 11 shows a representative sample of CNBP free of nucleic acid obtained from anion exchange chromatography (peak 3 of Fig. 2D). Molecular mass standards are indicated at the left of the figure. Expected positions of the Trx-His_6-TEV-CNBP fusion protein (37 kDa) and CNBP (18 kDa) are indicated at the right of the figure. (C) Average yield of different steps of the whole purification procedure expressed as mg per liter of initial culture and their concentrations as mg/ml. Trx-$CNBP_1$: Trx-His_6-TEV-CNBP fusion protein present in soluble culture extracts; Trx-$CNBP_2$: Trx-His_6-TEV-CNBP fusion protein present in elusions of the first Ni^{2+} chromatography; $CNBP_1$: CNBP obtained after TEV digestion; $CNBP_2$: CNBP present in the flow-through of the second Ni^{2+} chromatography; $CNBP_3$: CNBP free of nucleic acid obtained from anion exchange chromatography (peak 3 of Fig. 2D). Protein concentrations were calculated by absorption at 280 nm using the calculated CNBP molar extinction coefficient except for those samples indicated by (*), which were estimated by densitometry of the SDS–PAGE bands.

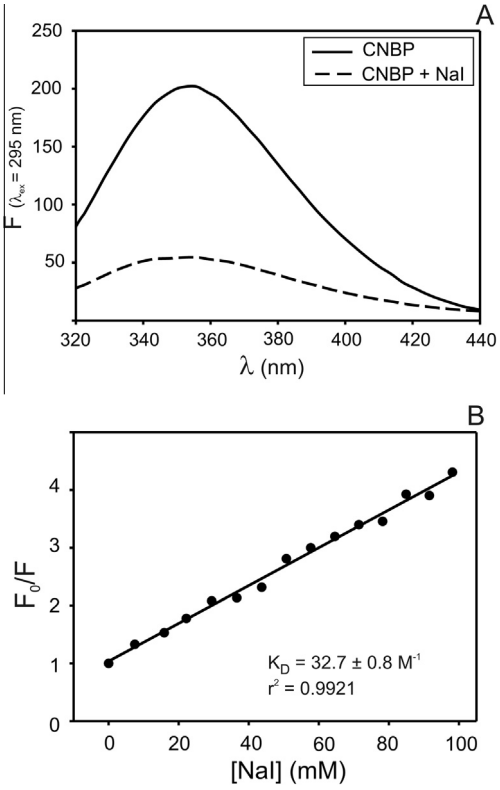

Fig. 5. Fluorescence quenching with iodide. (A) CNBP intrinsic tryptophan fluorescence emission spectrum shows a maximum at 352–357 nm. CNBP fluorescence was quenched by addition of NaI up to 100 mM. (B) Stern–Volmer plot of CNBP fluorescence quenching with iodide (λ_{ex} = 295 nm, the average fluorescence at λ_{em} = 352–357 nm was used). The Stern–Volmer constant of dynamic quenching (K_D) calculated from the linear regression fit was 32.7 ± 0.8 M^{-1}.

1 μM in 5 mM Tris–HCl pH 7.5, 20 mM NaCl, 1% Glycerol and 0.5 μM $ZnCl_2$. Secondary structure content was assigned by Dicroprot 2000 1.0.4 software [33] using K2D, Selcon 3 and Contin algorithms.

Proteolysis assays

Spontaneous proteolysis was assessed by incubating 30 μl of 0.2 μg/μl purified CNBP for different periods of time at 25 or 37 °C as indicated. Enzymatic proteolysis assays were carried out by addition of α-chymotrypsin to a 0.2 μg/μl CNBP solution using a protease/protein molar ratio of 1:80 and 5 mM $CaCl_2$ at 37° for different periods of time as indicated. Zinc depletion was performed by pre-incubating CNBP with 10 mM EDTA for 30 min at 37 °C. Nucleic acid relevance in CNBP protease resistance was analyzed by pre-incubating CNBP with equimolar ssDNA or RNA probes in the same conditions used for EMSAs (omitting BSA) for 30 min at 37 °C. Reactions were stopped by adding Sample Buffer for SDS–PAGE.

Results and discussion

Set-up of recombinant tag-free CNBP purification

Bearing in mind the high sensitivity of CNBP to proteases, we constructed a chimera by fusing the thioredoxin(Trx)-His_6 sequence provided by pET-32a(+) expression vector (Novagen, Inc.) to the zebrafish CNBP cDNA, linking both sequences by a sequence coding for a proteolytic site specifically recognized by the tobacco etch virus (TEV) protease [28] (Fig. 1B). The specificity of TEV is much higher than many other proteases commonly used [29], a fact that may avoid the proteolysis of CNBP N-terminal domain.

The Trx-His_6-TEV-CNBP fusion protein was expressed in *E. coli* and affinity purified using a Ni^{2+}-column. Subsequently, it was treated with TEV protease and then subjected to a second round of Ni^{2+}-column affinity chromatography so as to isolate CNBP from the Trx-His_6 product and TEV protease, as determined by western blot (Fig. S1). N-terminus sequencing revealed that purified CNBP contains an extra glycine residue at the N-terminus due to the TEV site insertion and proteolysis procedures (Fig. 1A).

The presence of multiple Zn knuckles in CNBP primary structure (Fig. 1A) led us to assess Zn^{2+} requirement during the expression procedure by adding 0.3 mM $ZnCl_2$ in the culture media. Electronic absorption spectroscopy of CNBP expressed in LB not supplemented with zinc (CNBP-LB) showed a typical protein maximum at 280 nm (Fig. 2A) whereas CNBP expressed in LB supplemented with Zn^{2+} (CNBP-LB-Zn) showed a broader signal shifted to lower wavelenghts with a maximum centered between 260 and 280 nm (Fig. 2B). Phenol:chloroform extraction and ethanol precipitation rendered a sample showing a typical nucleic acid spectrum (inset in Fig. 2B), suggesting that nucleic acids were co-purified with CNBP. Further anion exchange chromatography and electronic absorption spectroscopy showed that CNBP-LB eluted in two peaks (1 and 2 in Fig. 2C) with typical protein spectra and maxima at 280 nm (Fig. 2E). However, three elution peaks (3–5 in Fig. 2D) were observed for CNBP-LB-Zn. Peaks 3 and 4 showed

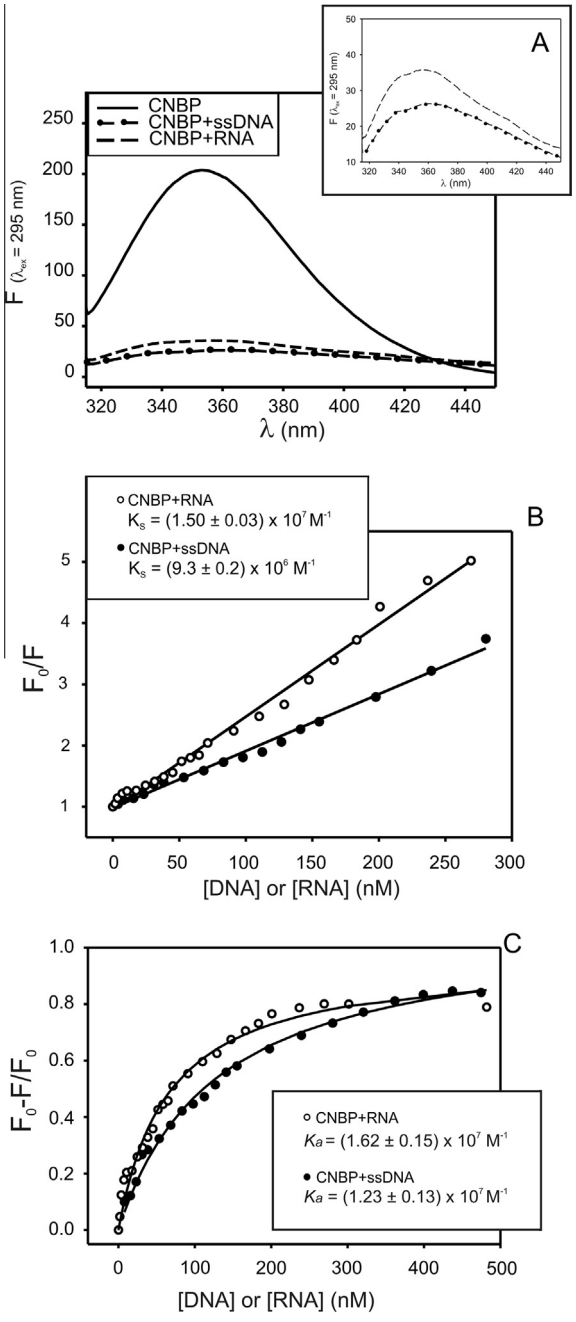

Fig. 6. Fluorescence quenching with nucleic acids. (A) CNBP intrinsic tryptophan fluorescence was notoriously quenched by addition of RNA and ssDNA. Inset shows fluorescence spectra of CNBP-ssDNA and CNBP-RNA titration endpoints. (B) Stern–Volmer plots of CNBP fluorescence quenching with nucleic acids (λ_{ex} = 295 nm, the average fluorescence at λ_{em} = 352–357 nm was used). Stern–Volmer constant of static quenching (K_S) were calculated from the slope of linear regression adjustments. (C) Relative quenching ΔF plots were used to calculate the CNBP affinity constants (K_a).

maxima at 280 nm whereas peak 5 showed a broad signal consistent with two overlapping peaks at 260 and 280 nm (Fig. 2F). SDS–PAGE and western blot showed that all fractions contained a unique ≈18 kDa polypeptide corresponding to CNBP (not shown). Differences in anion exchange chromatography elution profiles may be due to the presence of CNBP dimers or multimers, as previously suggested [10,25]. Therefore, aliquots containing CNBP at 5–30 μM from peaks 1 and 2 (for LB condition) or 3 and 4 (for LB-Zn condition) were chosen for further studies. Instead, CNBP eluted in peak 5 was not further used due to the probable co-purification with nucleic acids.

Table 2
Summary of association constants (K_a) calculated.

	EMSA (Fig. 3B and Fig. S2)		Fluorescence quenching plots (Fig. 6C)	
	RNA	ssDNA	RNA	ssDNA
CNBP LB-Zn	K_a = 3.1 (K_d = 0.32 μM)	K_a = 11 (K_d = 0.09 μM)	K_a = 12	K_a = 16
CNBP LB	K_a = 5.3 (K_d = 0.19 μM)	K_a = 3.0 (K_d = 0.33 μM)	nd	nd

All calculated association constants are expressed in μM^{-1} units. Calculation uncertainties are not reported here since they are informed in the referred figures. nd: not determined.

Zinc content was determined by atomic absorption spectroscopy yielding 5.8 Zn atoms per CNBP-LB molecule and 6.2 for CNBP-LB-Zn molecule. Despite this, CNBP expressed in LB-Zn was more stable to spontaneous proteolysis (Fig. 3A) and bound ssDNA in EMSA with higher affinity than CNBP expressed in LB (Fig. 3B, Table 1, and Fig. S2). Therefore, we included the addition of Zn^{2+} to the culture media as an experimental condition for CNBP expression. When we collated tag-free CNBP binding parameters obtained by EMSA against those ones obtained with tagged-CNBP, independently of the addition of Zn^{2+} to culture media, ssDNA or RNA were bound by GST-CNBP (Table 1 and Fig. S3) and His_6-CNBP (not shown) with lower affinity than tag-free CNBP. Although the presence of tags does not fully impair the CNBP binding capabilities, it is important to consider these issues when drawing conclusions about CNBP biological function.

The expression and purification protocol described here, summarized in Fig. 4A, was also used to obtain active homogeneously pure full-length human tag-free CNBP (not shown in this work). SDS–PAGE analysis of representative fractions of zebrafish CNBP purification is shown in Fig. 4B. Five mg of recombinant zebrafish CNBP were obtained from 1 L cultured *E. coli* cells at a concentration ≈0.2 mg/ml (Fig. 4C).

The achievement of tag-free CNBP allowed us to perform several biochemical and biophysical experimental approaches, as described below.

Biochemical characterization of CNBP

We next got insight into CNBP biochemical and structural characteristics by using several biochemical and biophysical methods, which could not be used before because of the presence of tags.

We employed fluorescence spectroscopy taking advantage of the unique and fully conserved tryptophan (Trp^{17}, Fig. 1A) [9]. Fluorescence emission spectra were performed exciting at 275, 280, or 295 nm (Fig. S4). We chose 295 nm as the excitation wavelength to avoid tyrosines excitation and fluorescence or energy transfer and inner filter effects due to nucleic acid absorbance. Emission spectra maxima were at 352–357 nm (Fig. 5A), suggesting that Trp^{17} is in a polar environment, likely exposed to the solvent. Trp^{17} fluorescence was quenched with sodium iodide, reaching background levels after addition of 100 mM NaI (Fig. 5A), further substantiating Trp^{17} exposure to the solvent. Stern–Volmer plot was linear (Fig. 5B), indicating the existence of a single fluorophore population accessible to iodide.

Addition of the ssDNA or RNA probes used for EMSA decreased Trp^{17} intrinsic fluorescence, reaching background levels upon the addition of 0.5 μM nucleic acid to a 3 μM CNBP solution (Fig. 6A). This finding suggests that Trp^{17} is directly involved in the binding of nucleic acids or, alternatively, that nucleic acid binding induces a conformational change that decreases Trp^{17} fluorescence. Stern–

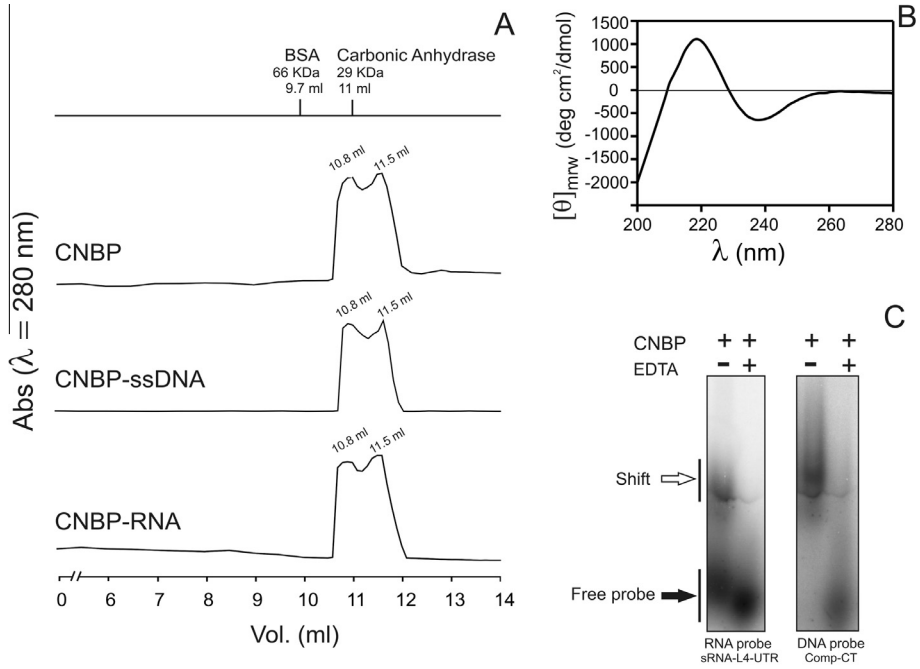

Fig. 7. CNBP structural characterization. (A) Elution profiles (280 nm absorbance) of size exclusion chromatographies (HPLC) of CNBP or CNBP pre-incubated with ssDNA or RNA. BSA and Carbonic Anhydrase were used as standards to assign the molecular size of each CNBP peak. (B) CNBP circular dichroism spectrum indicating the presence of 50% β-sheet structures and 50% of random-coil. (C) EMSAs performed with 2 nM labeled probe and 5 μM CNBP or 5 μM CNBP pre-incubated with 10 mM EDTA.

Volmer plots were linear (Fig. 6B) and with notoriously higher Stern–Volmer constants (K_S) than those obtained for titrations with iodide (K_D), indicating the presence of a unique fluorophore population quenched by nucleic acids, suggesting a static quenching with nucleic acids, and allowing the use of K_S as estimates of association constants.

Apparent association constants (K_a) estimated from EMSAs (Table 2) were used as initial parameters to fit the relative quenching data using a model that assumes equivalent and independent binding sites (Fig. 6C) [32]. K_a were in the same order of magnitude than those from EMSAs and than K_S obtained from Stern–Volmer plots (Table 2 and Fig. 6B).

Structural characterization of CNBP

CNBP structure was assessed by size-exclusion HPLC, circular dichroism (CD) spectroscopy, and controlled chymotrypsin proteolysis. Size-exclusion HPLC (Fig. 7A) revealed that CNBP possesses

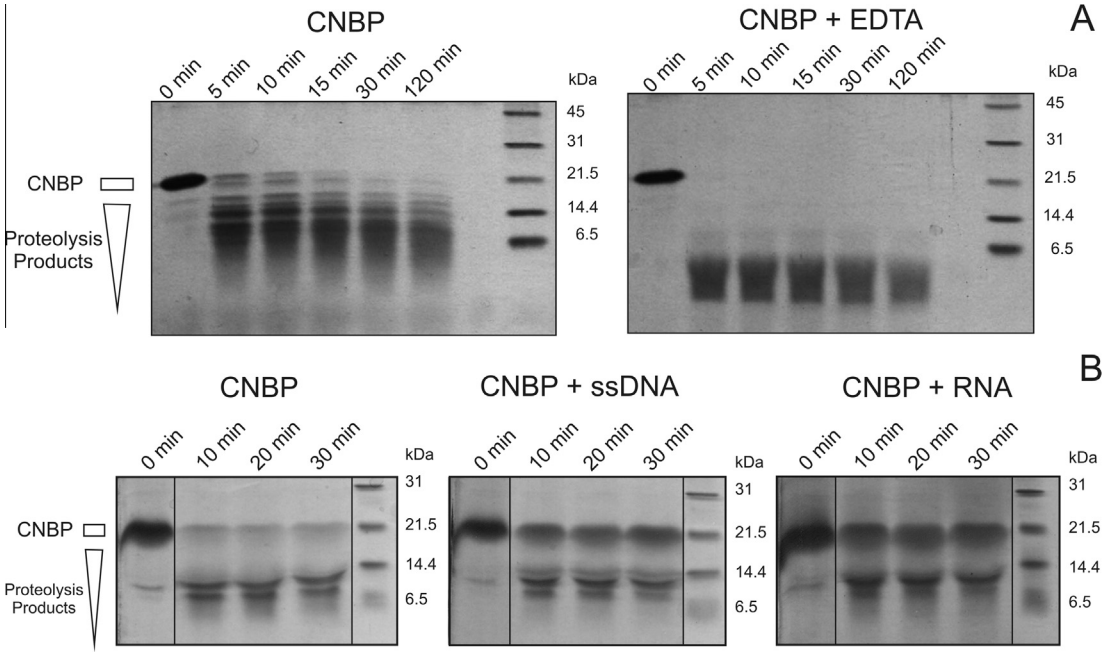

Fig. 8. Chymotrypsin proteolysis assays. (A) Proteolysis assays of CNBP and CNBP pre-incubated with 10 mM EDTA. (B) Proteolysis assays of CNBP and CNBP pre-incubated with ssDNA or RNA. Note that time periods of chymotrypsin assays (5–120 min) are much shorter than those of spontaneous proteolysis assays (6–24 h), thus avoiding interference of spontaneous proteolysis in the chymotrypsin assays. SDS–PAGEs were stained with Coomassie Brilliant Blue.

a quaternary structure consisting of homodimers coexisting with monomers either as non-interconvertible forms or in a very slow equilibrium that allowed their separation by size-exclusion HPLC, as well as by EMSA. Monomer an dimer peaks were similar in height and width, indicating that these species are present in a ≈1:1 mass ratio or ≈1:2 dimer/monomer molar ratio. The elution profile did not change after CNBP pre-incubation either with ssDNA or RNA in the same stoichiometric relationship used in end-points of fluorescence quenching titrations (Fig. 7A). This finding indicates that the relative proportion of monomer and dimer in solution is not affected by the nucleic acid binding, in agreement with previous reports [10,25] that had been carried out using tag-fused recombinant CNBP. Therefore, this is the first evidence that CNBP forms dimers by itself and independently of protein tags and nucleic acid binding.

CD spectra of tag-free CNBP showed one positive peak in the vicinity of 220 nm and one negative peak around 240 nm (Fig. 7B). Different software analyses predicted ≈50% β-sheet secondary structure and ≈50% random-coil. CNBP zinc knuckles are structurally and functionally analogous to zinc knuckles found in retroviral NCp [34,35], which consist of two short β-strands connected by a turn (β-hairpin) followed by a short loop [36–38]. Thus, the seven zinc knuckles structured around Zn^{2+} present in CNBP may account for the β-sheet structure predicted by CD. The 50% random-coil may correspond to the linkers between the seven zinc knuckles, the N- and C-terminal tails, and the naturally flexible RGG box, which collectively comprise ≈40% of CNBP amino acid sequence (Fig. 1A).

The contribution of zinc knuckle folding in CNBP structure and functionality was further assessed by employing Zn^{2+}-depleted CNBP in EMSA and proteolysis experiments. A marked decrease in CNBP binding to its targets in EMSA (Fig. 7C) and a higher sensitivity to time-dependent chymotrypsin proteolysis (Fig. 8A) were detected. The requirement of Zn^{2+} for CNBP binding to its ssDNA target had already been suggested by Michelotti and colleagues [23] who performed EMSA experiments using EGTA-treated nuclear extracts. However, here we report a direct implication of zinc in CNBP folding and binding to ssDNA and RNA using homogeneously pure protein.

Intrinsically unstructured nucleic acid chaperones usually fold upon binding to their biological targets [39–43]. Therefore, we hypothesized that CNBP gains structure upon binding to single-stranded nucleic acids. In support to this hypothesis, CNBP pre-incubated with its ssDNA or RNA targets was less sensitive to chymotrypsin time-dependent proteolysis (Fig. 8B), strongly suggesting that unstructured regions became ordered and, thus, less susceptible to protease activity.

Conclusions

We report a fast, simple and reproducible method for obtaining full length homogeneously pure and functional tag-free recombinant CNBP, which resulted suitable for biochemical and structural studies. Fluorescence spectroscopy revealed the presence of a unique and conserved tryptophan, which is exposed to the solvent and involved, directly or indirectly, in nucleic acid binding. Moreover, fluorescence quenching along with EMSA data enabled to better determine CNBP-nucleic acid association constants, found to be higher than those previously reported using CNBP fused to protein tags. Therefore, tag-free CNBP might be more appropriate to perform further biochemical studies.

Size-exclusion HPLC revealed that CNBP possesses a quaternary structure consisting of homodimers coexisting with monomers either as non-interconvertible forms or in a very slow equilibrium, and that dimers are formed regardless the presence of nucleic acid targets.

CD, EMSA, and proteolysis experiments showed that CNBP has a secondary structure dominated by β-sheet likely comprised by the zinc knuckles, and that folded zinc knuckles are required for CNBP stability and biochemical activity. Besides, an increase in structure stability was observed in the presence of CNBP-target single-stranded nucleic acids in a similar fashion than other unstructured nucleic acid chaperones.

These novel conclusions about CNBP structure and function were possible because of the availability of homogeneously pure, functional and tag-free CNBP. This reproducible purification method, together with the structural CNBP characterization reported here, will certainly result useful to shed light on the biological role of this strikingly conserved nucleic acid chaperone and probably other proteins with similar structural–functional features.

Acknowledgments

The present work was supported by Grants from ANPCyT (PICT 33299 and 00648 to NBC, PICT 00738 to PA, PICT 11-1540 to NBC and PA) and CONICET (PIP 00480 to PA, PIP 00773 to NBC and PA). PA, BBN, and NBC are staff members, EC is a fellow of CONICET and MNL is a former fellow of CONICET and a present Fondation pour la Recherche Médicale post-doctoral fellow at Institut Pasteur. We thank Enrique Morales, Salvador Peirú, Mariano Martinez, Daniela Albanesi, and Gabriela Coux for their technical support during protein purification and characterization. We also thank Marcela Culasso, María Robson, Mariana de Sanctis, and Geraldine Raimundo for editing this manuscript.

Appendix A. Supplementary data

Supplementary data associated with this article can be found, in the online version, at http://dx.doi.org/10.1016/j.pep.2013.10.006.

References

[1] C.L. Liquori, K. Ricker, M.L. Moseley, J.F. Jacobsen, W. Kress, S.L. Naylor, J.W. Day, L.P. Ranum, Myotonic dystrophy type 2 caused by a CCTG expansion in intron 1 of ZNF9, Science 293 (2001) 864–867.
[2] C. Schneider-Gold, L.T. Timchenko, CCUG repeats reduce the rate of global protein synthesis in myotonic dystrophy type 2, Rev. Neurosci. 21 (2010) 19–28.
[3] D.M. Niedowicz, T.L. Beckett, C.J. Holler, A.M. Weidner, M.P. Murphy, APP(DeltaNL695) expression in murine tissue downregulates CNBP expression, Neurosci. Lett. 482 (2010) 57–61.
[4] H.H. Chang, H.H. Hu, Y.J. Lee, H.M. Wei, M.C. Fan-June, T.C. Hsu, G.J. Tsay, C. Li, Proteomic analyses and identification of arginine methylated proteins differentially recognized by autosera from anti-Sm positive SLE patients, J. Biomed. Sci. 20 (2013) 27.
[5] A.M. Weiner, M.L. Allende, T.S. Becker, N.B. Calcaterra, CNBP mediates neural crest cell expansion by controlling cell proliferation and cell survival during rostral head development, J. Cell. Biochem. 102 (2007) 1553–1570.
[6] A.M. Weiner, N.L. Scampoli, N.B. Calcaterra, Fishing the molecular bases of treacher collins syndrome, PLoS ONE 7 (2012) e29574.
[7] A.M. Weiner, M.A. Sdrigotti, R.N. Kelsh, N.B. Calcaterra, Deciphering the cellular and molecular roles of cellular nucleic acid binding protein during cranial neural crest development, Dev. Growth Differ. 53 (2011) 934–947.
[8] P. Armas, T.H. Aguero, M. Borgognone, M.J. Aybar, N.B. Calcaterra, Dissecting CNBP, a zinc-finger protein required for neural crest development, in its structural and functional domains, J. Mol. Biol. 382 (2008) 1043–1056.
[9] N.B. Calcaterra, P. Armas, A.M. Weiner, M. Borgognone, CNBP: a multifunctional nucleic acid chaperone involved in cell death and proliferation control, IUBMB Life 62 (2010) 707–714.
[10] P. Armas, S. Nasif, N.B. Calcaterra, Cellular nucleic acid binding protein binds G-rich single-stranded nucleic acids and may function as a nucleic acid chaperone, J. Cell. Biochem. 103 (2008) 1013–1036.
[11] P. Armas, E. Margarit, V.S. Mouguelar, M.L. Allende, N.B. Calcaterra, Beyond the binding site: in vivo identification of tbx2, smarca5 and wnt5b as molecular targets of CNBP during embryonic development, PLoS ONE 8 (2013) e63234.
[12] M.A. Sammons, A.K. Antons, M. Bendjennat, B. Udd, R. Krahe, A.J. Link, ZNF9 activation of IRES-mediated translation of the human ODC mRNA is decreased in myotonic dystrophy type 2, PLoS ONE 5 (2010) e9301.

[13] S. Schlatter, M. Fussenegger, Novel CNBP- and La-based translation control systems for mammalian cells, Biotechnol. Bioeng. 81 (2003) 1–12.
[14] C. Huichalaf, B. Schoser, C. Schneider-Gold, B. Jin, P. Sarkar, L. Timchenko, Reduction of the rate of protein translation in patients with myotonic dystrophy 2, J. Neurosci. 29 (2009) 9042–9049.
[15] M.A. Sammons, P. Samir, A.J. Link, Saccharomyces cerevisiae Gis2 interacts with the translation machinery and is orthogonal to myotonic dystrophy type 2 protein ZNF9, Biochem. Biophys. Res. Commun. 406 (2011) 13–19.
[16] T. Scherrer, C. Femmer, R. Schiess, R. Aebersold, A.P. Gerber, Defining potentially conserved RNA regulons of homologous zinc-finger RNA-binding proteins, Genome Biol. 12 (2011) R3.
[17] V.R. Gerbasi, A.J. Link, The myotonic dystrophy type 2 protein ZNF9 is part of an ITAF complex that promotes cap-independent translation, Mol. Cell. Proteomics 6 (2007) 1049–1058.
[18] N.B. Calcaterra, J.F. Palatnik, D.M. Bustos, S.E. Arranz, M.O. Cabada, Identification of mRNA-binding proteins during development: characterization of Bufo arenarum cellular nucleic acid binding protein, Dev. Growth Differ. 41 (1999) 183–191.
[19] P. Armas, M.O. Cabada, N.B. Calcaterra, Primary structure and developmental expression of Bufo arenarum cellular nucleic acid-binding protein: changes in subcellular localization during early embryogenesis, Dev. Growth Differ. 43 (2001) 13–23.
[20] P. Armas, S. Cachero, V.A. Lombardo, A. Weiner, M.L. Allende, N.B. Calcaterra, Zebrafish cellular nucleic acid-binding protein: gene structure and developmental behaviour, Gene 337 (2004) 151–161.
[21] M. Borgognone, P. Armas, N.B. Calcaterra, Cellular nucleic-acid-binding protein, a transcriptional enhancer of c-Myc, promotes the formation of parallel G-quadruplexes, Biochem. J. 428 (2010) 491–498.
[22] V.A. Lombardo, P. Armas, A.M. Weiner, N.B. Calcaterra, In vitro embryonic developmental phosphorylation of the cellular nucleic acid binding protein by cAMP-dependent protein kinase, and its relevance for biochemical activities, FEBS J. 274 (2007) 485–497.
[23] E.F. Michelotti, T. Tomonaga, H. Krutzsch, D. Levens, Cellular nucleic acid binding protein regulates the CT element of the human c-myc protooncogene, J. Biol. Chem. 270 (1995) 9494–9499.
[24] L. Pellizzoni, F. Lotti, B. Maras, P. Pierandrei-Amaldi, Cellular nucleic acid binding protein binds a conserved region of the 5′UTR of Xenopus laevis ribosomal protein mRNAs, J. Mol. Biol. 267 (1997) 264–275.
[25] L. Pellizzoni, F. Lotti, S.A. Rutjes, P. Pierandrei-Amaldi, Involvement of the Xenopus laevis Ro60 autoantigen in the alternative interaction of La and CNBP proteins with the 5′UTR of L4 ribosomal protein mRNA, J. Mol. Biol. 281 (1998) 593–608.
[26] S. Chen, L. Su, J. Qiu, N. Xiao, J. Lin, J.H. Tan, T.M. Ou, L.Q. Gu, Z.S. Huang, D. Li, Mechanistic studies for the role of cellular nucleic-acid-binding protein (CNBP) in regulation of c-myc transcription, Biochim. Biophys. Acta 2013 (1830) 4769–4777.
[27] J. Arnau, C. Lauritzen, G.E. Petersen, J. Pedersen, Current strategies for the use of affinity tags and tag removal for the purification of recombinant proteins, Protein Expr. Purif. 48 (2006) 1–13.
[28] J.C. Carrington, W.G. Dougherty, A viral cleavage site cassette: identification of amino acid sequences required for tobacco etch virus polyprotein processing, Proc. Natl. Acad. Sci. USA 85 (1988) 3391–3395.
[29] J. Phan, A. Zdanov, A.G. Evdokimov, J.E. Tropea, H.K. Peters III, R.B. Kapust, M. Li, A. Wlodawer, D.S. Waugh, Structural basis for the substrate specificity of tobacco etch virus protease, J. Biol. Chem. 277 (2002) 50564–50572.
[30] S.C. Gill, P.H. von Hippel, Calculation of protein extinction coefficients from amino acid sequence data, Anal. Biochem. 182 (1989) 319–326.
[31] U.K. Laemmli, Cleavage of structural proteins during the assembly of the head of bacteriophage T4, Nature 227 (1970) 680–685.
[32] J. Wyman, S.J. Gill, Binding and Linkage. Functional Chemistry of Biological Macromolecules, University Science Books, Mill Valley, 1990.
[33] G. Deleage, C. Geourjon, An interactive graphic program for calculating the secondary structure content of proteins from circular dichroism spectrum, Comput. Appl. Biosci. 9 (1993) 197–199.
[34] C.F. McGrath, J.S. Buckman, T.D. Gagliardi, W.J. Bosche, L.V. Coren, R.J. Gorelick, Human cellular nucleic acid-binding protein Zn2+ fingers support replication of human immunodeficiency virus type 1 when they are substituted in the nucleocapsid protein, J. Virol. 77 (2003) 8524–8531.
[35] P. Armas, N.B. Calcaterra, Retroviral zinc knuckles in eukaryotic cellular proteins, in: R. Ciofani, L. Makrlík (Eds.), Zinc Fingers: Structure, Properties and Applications, Nova Science Publishers Inc., Hauppauge NY, 2012, pp. 51–80.
[36] T.L. South, P.R. Blake, D.R. Hare, M.F. Summers, C-terminal retroviral-type zinc finger domain from the HIV-1 nucleocapsid protein is structurally similar to the N-terminal zinc finger domain, Biochemistry 30 (1991) 6342–6349.
[37] N. Morellet, N. Jullian, H. de Rocquigny, B. Maigret, J.L. Darlix, B.P. Roques, Determination of the structure of the nucleocapsid protein NCp7 from the human immunodeficiency virus type 1 by 1H NMR, EMBO J. 11 (1992) 3059–3065.
[38] M.F. Summers, T.L. South, B. Kim, D.R. Hare, High-resolution structure of an HIV zinc fingerlike domain via a new NMR-based distance geometry approach, Biochemistry 29 (1990) 329–340.
[39] R. Ivanyi-Nagy, L. Davidovic, E.W. Khandjian, J.L. Darlix, Disordered RNA chaperone proteins: from functions to disease, Cell. Mol. Life Sci. 62 (2005) 1409–1417.
[40] P.E. Wright, H.J. Dyson, Linking folding and binding, Curr. Opin. Struct. Biol. 19 (2009) 31–38.
[41] H.J. Dyson, P.E. Wright, Coupling of folding and binding for unstructured proteins, Curr. Opin. Struct. Biol. 12 (2002) 54–60.
[42] P. Tompa, P. Csermely, The role of structural disorder in the function of RNA and protein chaperones, FASEB J. 18 (2004) 1169–1175.
[43] P. Tompa, The interplay between structure and function in intrinsically unstructured proteins, FEBS Lett. 579 (2005) 3346–3354.